Supporting Information to the article: A polarizable force field for computing the infra-red spectra of the polypeptide backbone

Verena Schultheis, Rudolf Reichold, Bernhard Schropp, and Paul Tavan*

Lehrstuhl für Biomolekulare Optik, Ludwig-Maximilians-Universität,

Oettingenstr. 67, 80538 München, Germany

*email: tavan@physik.uni-muenchen.de; phone: +49-89-2180-9220

The sets of graphs in Figs. 12 and 13 document the results of the MT/BP calculations on NMA exposed to homogeneous electric fields E_j oriented along the axes $j \in \{x, y, z\}$ of the Cartesian coordinate system depicted in Fig. 2. Field dependent equilibrium values of the internal coordinates depicted in Fig. 3 were taken directly from NMA's equlibrium geometries $\mathcal{G}(E_j)$, whereas harmonic force constants $k_i(E_j)$ were derived from the MT/BP Hessians $\mathbf{H}(E_j)$ through the iterative match of intrinsic frequencies explained in Sec. 2.2. The graphs contain linear fits to the MT/BP derived force field parameters whose slopes give the linear response parameters in Tab. 4. Some of the deviations from linearity occurring at very large fields are computational artifacts of the MT/BP approach associated with a field-induced pushing of electron density towards the boundaries of the DFT box, whithin which that density is expanded into plane waves.

Fig. 14 serves to illustrate the difference between the simple AG force field defined by Eqs. (2) and (4) and a DFT force field. By visually subtracting the nearly diagonal MM(DFT) Hessian in (B) from the DFT reference in (A) one can get clues, which of the neglected coupling terms given by Eq. (6) are important for the computation of correct frequencies.

Fig. 15 demonstrates that most parts of the IR spectra of protonated and deuterated NMA in aqueous solution, which were derived by FTTCF from extended DFT/MM-MD simulations, are quite well converged. Mainly the regions of the AI bands exhibit larger differences in spectral shape when computed from the first 26 ps (red) and all 78 ps (blue) of the simulations. We suspect that in both cases the respective system was not yet sufficiently equilibrated at the beginning of the production run.

Fig. 16 shows for the case of protonated NMA that the effects of hydrogen bonding on solvatochromic band shifts are small. See the caption to this figure and the discussion of the dashed line in Fig. 11D.

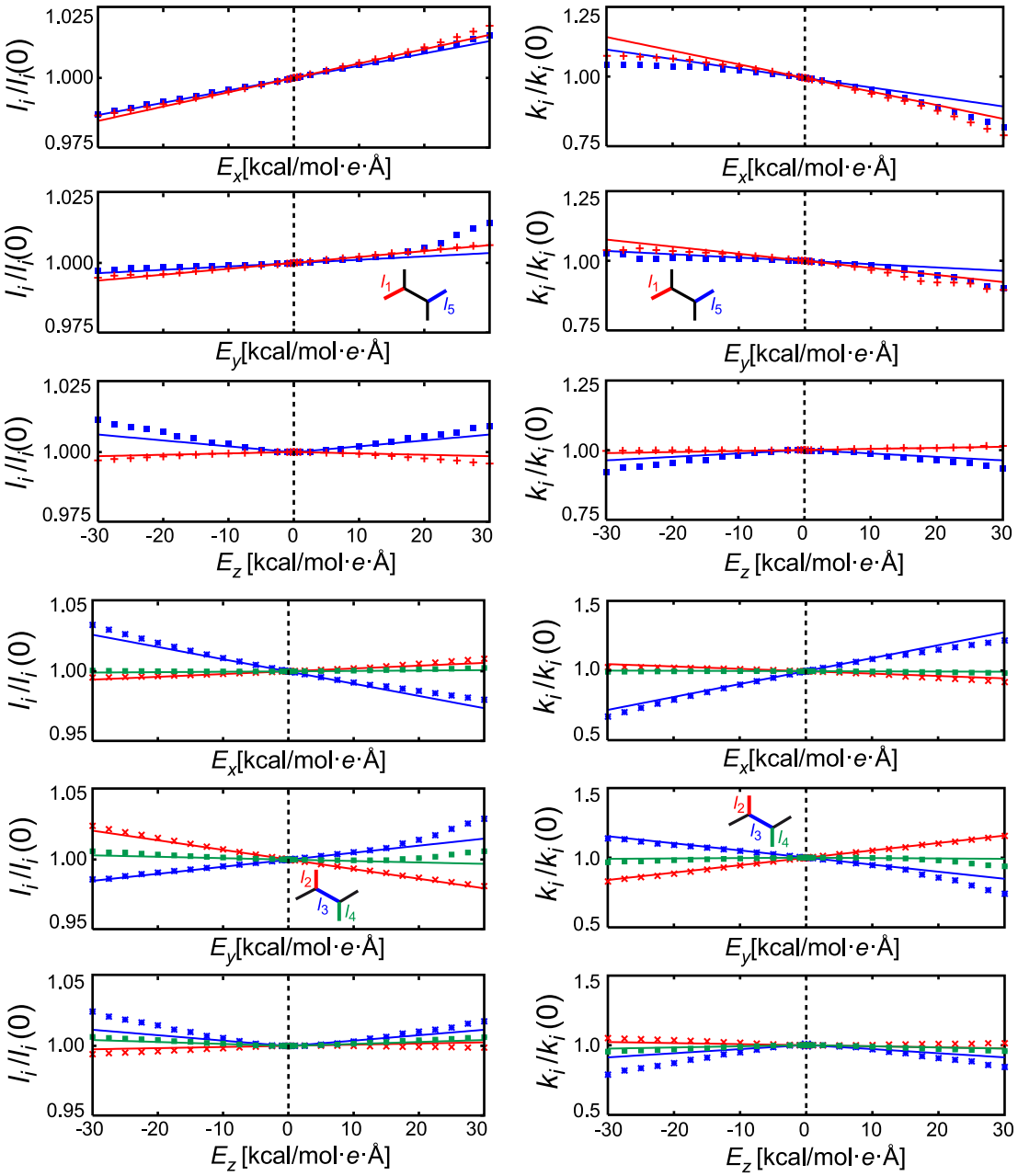

Figure 12: MT/BP equilibrium bond lengths $l_i(\mathbf{E})/l_i(0)$ (left) and force constants $k_i(\mathbf{E})/k_i(0)$ (right) as functions of electric fields E_x, E_y, E_z; solid lines are linear fits to data for fields in the range $[-10, 10]$ kcal/(mol Å e).

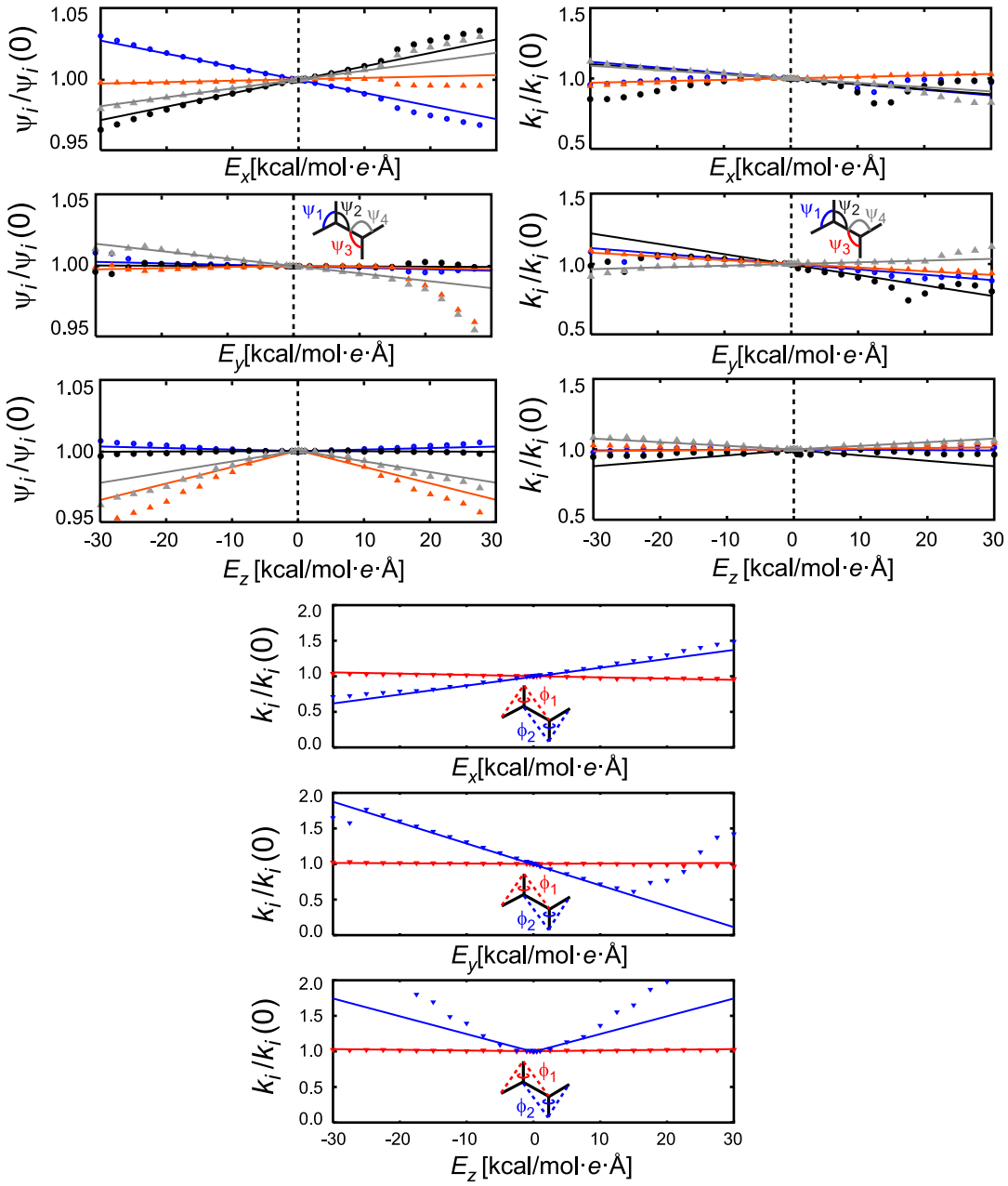

Figure 13: MT/BP equilibrium bond angles $\psi_i(\mathbf{E})/\psi_i(0)$ (top left), associated force constants $k_i(\mathbf{E})/k_i(0)$ (top right) and force constants of improper dihedral angles $\phi_i(\mathbf{E})/\phi_i(0)$ as functions of electric fields E_x, E_y, E_z and associated linear fits.

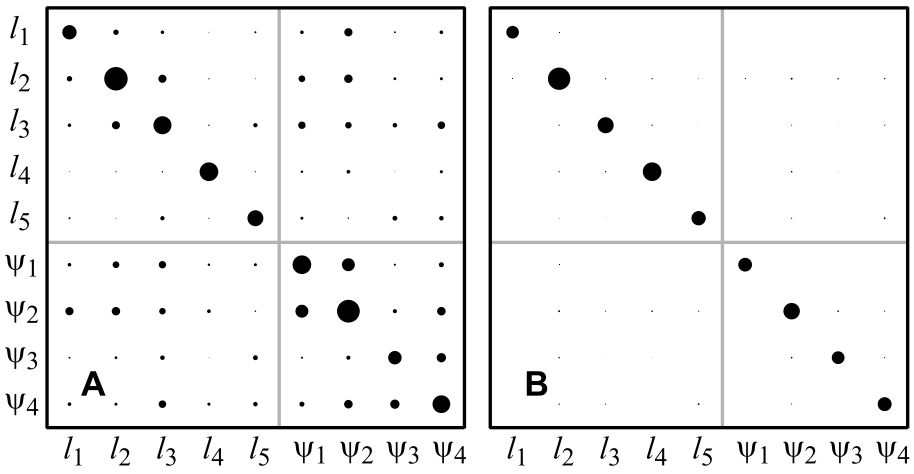

Figure 14: Structure of Hessian matrices in internal coordinates from (A) DFT and (B) MM(DFT) force fields for isolated NMA molecules. Absolute values of matrix elements are coded by circle sizes. The small off-diagonal terms in (B) are due to small so-called non-bonded interactions within NMA.

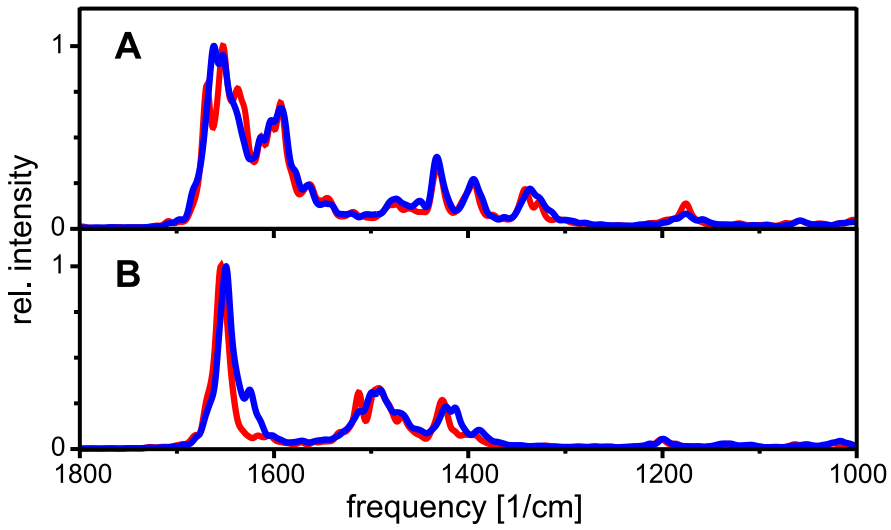

Figure 15: Convergence of solution spectra for (A) protonated and (B) deuterated NMA. FTTCF spectra from DFT/MM-MD trajectories of different lengths are compared: First 26 ps (red), and all 78 ps (blue). Frequencies are scaled by a factor of 1.0354. Intensities are normalized to the respective maximum values.

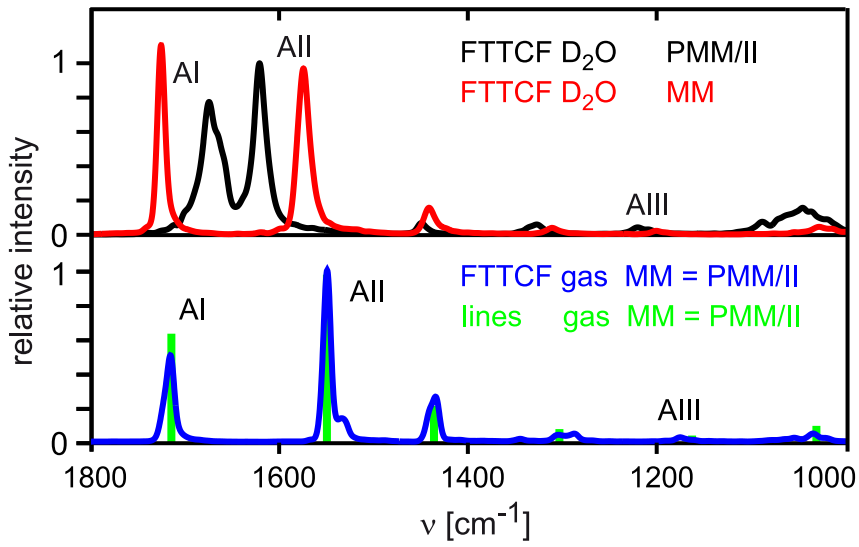

Figure 16: Comparison of FTTCF spectra calculated for protonated NMA in D_2O and in the gas phase (bottom) with different MM force fields from MD trajectories. By comparing the MM result for D_2O (red) with that for the gas phase (blue) one gets a clue on the effects of hydrogen bonding, by comparing with the PMM/II result for D_2O (black) one recognizes the effects of bond polarization. For the gas phase the MM(DFT) line spectrum obtained from normal mode analysis is also given. Frequencies are scaled by a factor of 0.9925.

The remaining Figs. 17, 18, and Tab. 5 document a failed attempt to construct a PMM/II force field for AGs, which performs better at least on the frequencies of the AI-AIII modes while retaining the quality of the mode description achieved with the force field MM(DFT). In this attempt we considered the force constants of the ICs as adjustable parameters and tried to optimize by gradient descent the deviation measure Eq. (10) defined further below (using the index sets $\mathcal{I} = \{1, \ldots, 6\}$ and $\mathcal{J} = \{7, 8, 9\}$).

The modified force constants obtained by these gradient descent procedures are listed in Tab. 5 under the labels $\mathrm{MM_{o1}}$(DFT) and $\mathrm{MM_{o2}}$(DFT) together with the starting values MM(DFT). By construction the optimized force fields closely reproduce the MT/BP spectrum of the "AG within NMA" in the high frequency region as can be seen by comparing the corresponding columns in Fig. 17. On the other hand, according to Fig. 18 the frequency-optimized force fields $\mathrm{MM_{o1/2}}$(DFT) now predict for the normal modes AI-AIII compositions, which sizably deviate from the MT/BP references. Thus by a tuning of the harmonic force constants one can reach an excellent match of selected frequencies while loosing the perfect match of the corresponding normal mode compositions. As a result the inclusion of the cross terms (5) cannot be avoided for an improved frequency matching that retains good quality mode compositions.

In our frequency optimizations we used the weighted deviation measure

$$\langle \Delta\nu^2 \rangle_{\mathcal{I}}^{\mathcal{J}} = \sqrt{\frac{\sum_{i\in\mathcal{I}} \Delta\nu_i^2 + (\sum_{i\in\mathcal{J}} \Delta\nu_i^2)/20}{|\mathcal{I}| + |\mathcal{J}|/20}} \tag{10}$$

where $\mathcal{I}$ and $\mathcal{J}$ are two sets of indices. The frequencies ν_i, $i \in \mathcal{I}$, fully contribute to this deviation whereas frequencies ν_i, $i =\in \mathcal{J}$ only contribute with a weight reduced by a factor 1/20. This measure takes all frequencies into account but is mainly determined by frequencies with indices $i \in \mathcal{I}$.

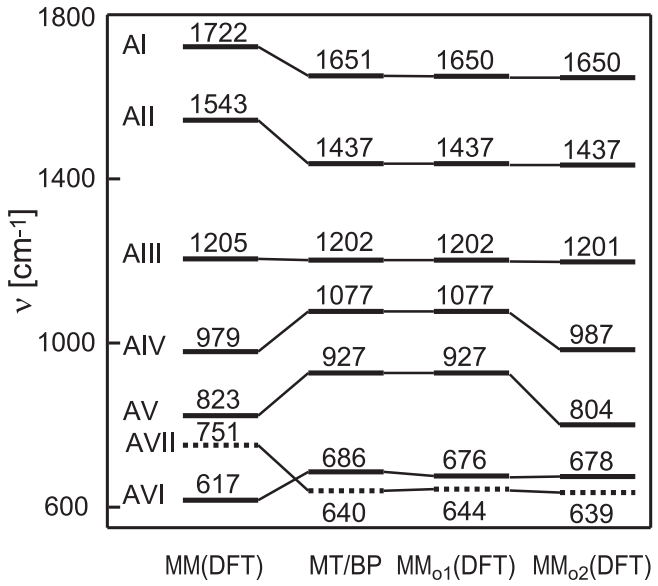

Figure 17: MT/BP spectra of the "AG within NMA" (defined by methyl groups with nearly massless hydrogen atoms, cf. Sec. 4.3) compared with MM spectra calculated at different parameterizations. The employed parameter sets MM(DFT), MM_{o1}(DFT), and MM_{o2}(DFT) are listed in the corresponding columns of Tab. 5 and are explained in the text. For line styles and mode labels see the caption to Fig. 4.

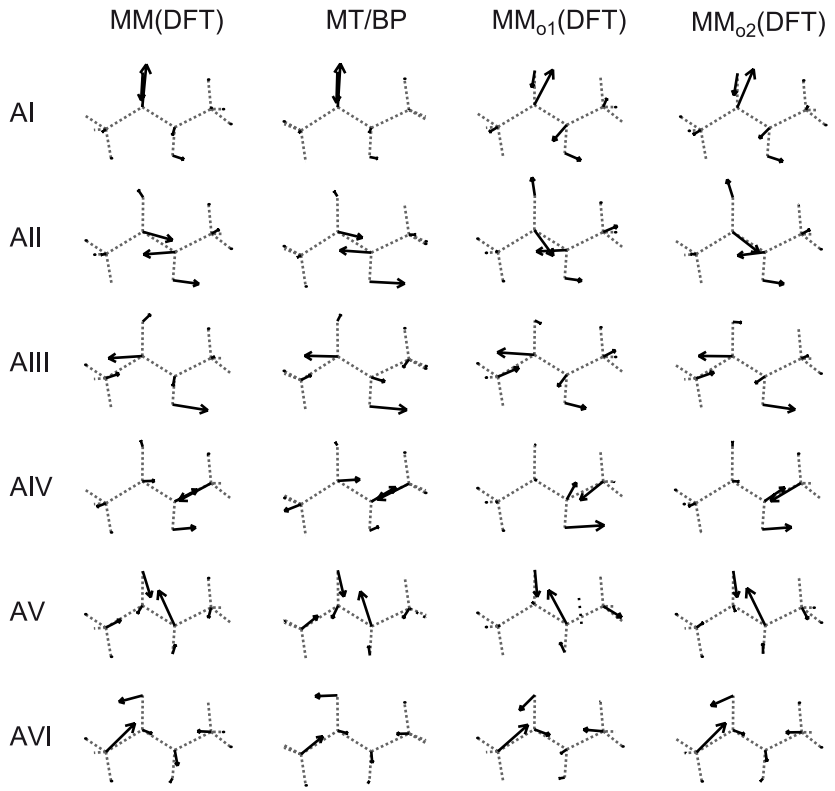

Figure 18: In-plane normal modes of the "AG within NMA" (cf. Sec. 4.3) belonging to the line spectra depicted in Fig. 17. Dashed lines indicate the bonds within the NMA molecule covering the AG depicted in Fig. 3. Arrows indicate atomic motions.

Table 5: Harmonic zero-field parameters of an AG.

		MM(DFT)	MM_{o1}(DFT)	MM_{o2}(DFT)
q_i	q_i^0	k_i	k_i	k_i
l_1	1.520 Å	460*	629*	577*
l_2	1.233 Å	1443*	1075*	1214*
l_3	1.374 Å	748*	543*	490*
l_4	1.015 Å	1009*	1004*	1006*
l_5	1.455 Å	591*	781*	604*
ψ_1	121.9 deg	4.7$	4.2$	5.6$
ψ_2	122.6 deg	6.9$	5.1$	7.4$
ψ_3	118.5 deg	4.2$	3.8$	3.9$
ψ_4	122.5 deg	4.9$	14.2$	7.3$
ϕ_1	0 deg	7.1$	4.9$	4.9$
ϕ_2	0 deg	1.2$	1.1$	1.1$
ξ	180 deg	0.8$	0.8$	0.8$

*[kcal/(mol Å^2)], $[kcal/{mol (10 deg)^2}].